Attractive Coulomb interaction of two-dimensional Rydberg excitons

V. Shahnazaryan,[1,2,3] I. A. Shelykh,[1,3,4] and O. Kyriienko[5]

[1]*Science Institute, University of Iceland, Dunhagi-3, IS-107 Reykjavik, Iceland*

[2]*Institute of Mathematics and High Technologies, Russian-Armenian (Slavonic) University, Hovsep Emin 123, 0051 Yerevan, Armenia*

[3]*Department of Photonics and Optical Information, ITMO University, St. Petersburg 197101, Russia*

[4]*Division of Physics and Applied Physics, Nanyang Technological University, 637371 Singapore*

[5]*The Niels Bohr Institute, University of Copenhagen, Blegdamsvej 17, DK-2100 Copenhagen, Denmark*

(Received 18 January 2016; revised manuscript received 14 May 2016; published 7 June 2016)

We analyze theoretically the Coulomb scattering processes of highly excited excitons in the direct-band-gap semiconductor quantum wells. We find that contrary to the interaction of ground-state excitons, the electron and hole exchange interaction between excited excitons has an attractive character both for s- and p-type two-dimensional (2D) excitons. Moreover, we show that similar to the three-dimensional highly excited excitons, the direct interaction of 2D Rydberg excitons exhibits van der Waals–type long-range interaction. The results predict the linear growth of the absolute value of exchange interaction strength with an exciton principal quantum number and point the way towards enhancement of optical nonlinearity in 2D excitonic systems.

DOI: 10.1103/PhysRevB.93.245302

I. INTRODUCTION

The possibility to attain strong and tunable interparticle interactions in a many-body system is indispensable for both fundamental studies of strong correlations and practical exploitation of nonlinear effects. The vast variety of collective effects in cold-atom systems [1] has profited from the usage of Feshbach resonances [2]. They allow for tunability of the s-wave scattering length for atomic collisions, changing the interaction character from a short-range repulsive one to an attractive one. A major step forward in boosting the atomic interaction strength can be performed when atoms are excited to a large principal quantum number Rydberg state [3]. In this case the absolute value of the interaction strength grows dramatically, and the interaction potential becomes of long range type, leading to the phenomenon of the Rydberg blockade [4–6]. This facilitates numerous applications in the quantum optics domain [7], where large effective nonlinearity for photons enables efficient photon crystallization [8], creation of photonic molecules [9], ordered pattern formation [10], etc.

In the solid-state physics, studies of many-body effects and nonlinear quantum optics became possible for systems of interacting quasiparticles typically probed by light. Here, the prominent examples are indirect excitons [11,12] and exciton polaritons [13]. The latter quasiparticles formed by the microcavity photons and excitons in a two-dimensional (2D) semiconductor quantum well (QW) are especially valuable for observing nonequilibrium condensation [14,15], vortices [16], solitons [17,18], and other effects characteristic of a weakly nonlinear Bose gas. At the same time, the highly anticipated transition of polaritonics to the quantum nonlinear regime is deferred by small and short-range exciton-exciton interaction in QWs, which are dominated by *repulsive* Coulomb exchange, while the direct-interaction contribution is negligible [19,20], except for the narrow energy range where the formation of the bipolariton is possible. Therefore, it opens the challenge for system modification to attain strong interaction, or, alternatively, the search for optional strategies which require only weak nonlinearity [21–23].

Up-to-date proposals for the enhancement of nonlinearity include hybridization of polaritons with dipolar excitons (dipolaritons) [24–26] and exploitation of the biexcitonic Feshbach resonance [27,28], although with limited capabilities. A drastic improvement was made in the system of highly excited three-dimensional (3D) excitons, which is the excitonic counterpart of Rydberg atoms physics [29]. In [29] the authors reported an observation of the dipolar blockade appearing in bulk Cu_2O for giant excitons with a principal quantum number up to $n = 25$ and a micron diameter. The important consequence of using this rather peculiar copper oxide semiconductor is selection rules which allow to optically pump excitons in the p state, where excitons exhibit the long-range interaction of dipolar and van der Waals types, similar to Rydberg atoms. At the same time, while results show the potential for strongly nonlinear optics, the requirement of 3D geometry and the infeasibility of Cu_2O-based microcavities hinder its application in the conventional form.

In this paper we pose the question of the possible achievement of the strong exciton-exciton interaction exploiting highly excited states of excitons in 2D semiconductor quantum wells. We show that for small transferred momenta the interaction of 2D excitons is dominated by a short-range exchange Coulomb interaction for both s and p exciton types, and we find that for excitons with a higher than ground principal quantum number ($n > 1$) the interaction constant changes sign, leading to an *attractive* exciton-exciton potential. The absolute value of the interaction strength scales linearly with n and increases for narrow-band-gap semiconductors. At the same time, similar to the 3D geometry, the direct interaction of 2D excitons possesses a long-range nature governed by van der Waals' law and grows drastically with n. This suggests that a 2D Rydberg exciton gas represents the nontrivial system and can lead to the emergence of hybrid repulsive-attractive bosonic mixtures.

II. THE MODEL

The calculation of the interaction potential for 2D excitons in the ground state can be done within the Coulomb scattering

formalism [19]. The theory can be extended to describe the interaction of excitons in the excited states. The two-dimensional exciton wave function with in-plane wave vector $\mathbf{Q}$ in the general form reads

$$\Psi_{\mathbf{Q},n,m}(\mathbf{r}_e,\mathbf{r}_h) = \frac{1}{\sqrt{A}} \exp[i\mathbf{Q}(\beta_e\mathbf{r}_e + \beta_h\mathbf{r}_h)]\psi_{n,m}(|\mathbf{r}_e - \mathbf{r}_h|), \tag{1}$$

where $\mathbf{r}_e,\mathbf{r}_h$ are in-plane radius vectors of electron and hole, respectively, and A denotes the normalization area. The coefficients β_e,β_h are defined as $\beta_{e(h)} = m_{e(h)}/(m_e + m_h)$, where $m_{e(h)}$ is the mass of an electron (hole). The internal relative motion is described by [30]

$$\begin{aligned}\psi_{n,m}(|\mathbf{r}_e - \mathbf{r}_h|) &= \frac{1}{\sqrt{2}\lambda_{2D}}\sqrt{\frac{(n-|m|-1)!}{(n-1/2)^3(n+|m|-1)!}}\left(\frac{|\mathbf{r}_e-\mathbf{r}_h|}{(n-1/2)\lambda_{2D}}\right)^{|m|} \\ &\times \exp\left[-\frac{|\mathbf{r}_e-\mathbf{r}_h|}{(2n-1)\lambda_{2D}}\right] L^{2|m|}_{n-|m|-1}\left[\frac{|\mathbf{r}_e-\mathbf{r}_h|}{(n-1/2)\lambda_{2D}}\right] \\ &\times \frac{1}{\sqrt{2\pi}} e^{im\varphi},\end{aligned} \tag{2}$$

where $n = 1,2,3,\ldots$ is the principal quantum number, $m = 0,\pm 1,\ldots,\pm n \mp 1$ is the magnetic quantum number, and λ_{2D} is a variational parameter related to the two-dimensional radius of the ground-state exciton. Here, $L^k_n[x]$ denotes the associated Laguerre polynomial. In the following we consider the narrow quantum well limit and thus disregard exciton motion in the confinement direction.

Considering excitons with only the parallel spin, the process of Coulomb scattering in reciprocal space associated with the transfer of wave vector $\mathbf{q}$ can be described by the form

$$(n,m,\mathbf{Q}) + (n',m,\mathbf{Q}') \to (n,m,\mathbf{Q}+\mathbf{q}) + (n',m,\mathbf{Q}'-\mathbf{q}). \tag{3}$$

The scattering matrix element consists of four terms:

$$H(n,n',m,\Delta\mathbf{Q},\mathbf{q},\beta_e) = \frac{e^2}{4\pi\varepsilon\varepsilon_0}\frac{\lambda_{2D}}{A} I_{\text{tot}}(n,n',m,\Delta\mathbf{Q},\mathbf{q},\beta_e), \tag{4}$$

where

$$\begin{aligned}I_{\text{tot}}(n,n',m,\Delta\mathbf{Q},\mathbf{q},\beta_e) &= I_{\text{dir}}(n,n',m,\mathbf{q},\beta_e) + I^X_{\text{exch}}(n,n',m,\Delta\mathbf{Q},\mathbf{q},\beta_e) \\ &+ I^e_{\text{exch}}(n,n',m,\Delta\mathbf{Q},\mathbf{q},\beta_e) + I^h_{\text{exch}}(n,n',m,\Delta\mathbf{Q},\mathbf{q},\beta_e).\end{aligned} \tag{5}$$

Here, the first term denotes the direct-interaction integral, the second corresponds to the exciton exchange interaction, and the last two terms describe electron and hole exchange integrals (see Appendix A for definitions and details).

Note that in the particular case where the wave vectors and principal quantum numbers of excitons coincide, $\Delta Q = |\mathbf{Q}-\mathbf{Q}'| = 0$ and $n = n'$, we have

$$I^X_{\text{exch}}(n,n,m,0,\mathbf{q},\beta_e) = I_{\text{dir}}(n,n,m,\mathbf{q},\beta_e), \tag{6}$$

$$I^e_{\text{exch}}(n,n,m,0,\mathbf{q},\beta_e) = I^h_{\text{exch}}(n,n,m,0,\mathbf{q},\beta_e), \tag{7}$$

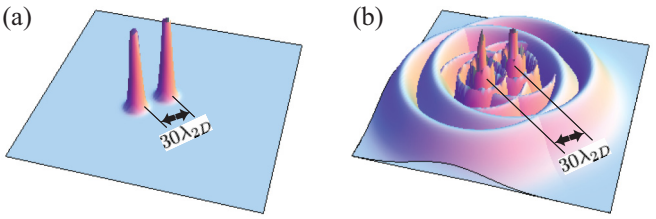

FIG. 1. Real-space distribution of exciton envelope wave functions with center-to-center separation distance of $30\lambda_{2D}$, shown for excitons in (a) the $1s$ state and (b) the $6s$ state.

and consequently,

$$I_{\text{tot}}(n,m,\mathbf{q},\beta_e) = 2\big[I_{\text{dir}}(n,m,\mathbf{q},\beta_e) + I^e_{\text{exch}}(n,m,\mathbf{q},\beta_e)\big]. \tag{8}$$

In the following we are interested in the dependence of the interaction on the scattered momentum $\mathbf{q}$, while considering equal exciton center-of-mass momenta, $\Delta Q = 0$.

To gain a qualitative understanding of interaction processes for highly excited excitons we shall look at the large-n exciton wave function. In particular, Eq. (2) implies that the spatial distribution of the exciton drastically increases with the principal quantum number. Namely, the higher the principal number of excitation is, the larger the spread of the wave function is, providing increased overlap between excitons and, consequently, leading to the enhanced exciton-exciton interaction. In Fig. 1(a) the real-space distribution of two excitons in the ground state is presented, where the interexciton distance is fixed to $30\lambda_{2D}$. The peak-shaped distribution of the wave functions determines the interaction behavior, which rapidly decreases as distance grows. Figure 1(b) shows the probability distribution for excitons in the $6s$ state, with the same interexciton distance as before (i.e., the same density of particles), revealing a large overlap of wave functions.

III. RESULTS

A. Interaction between s-type excitons

We examined numerically the Coulomb interaction integrals between excitons in the s and p states as a function of the scattered momentum $\mathbf{q}$. The calculation was done by multi-dimensional Monte Carlo integration while implementing the importance sampling algorithm, provided by the numerical integration CUBA library [31]. To be specific, we fixed the electron-to-exciton mass ratio to the value $\beta_e = 0.4$, which is close to the GaAs quantum well effective-mass ratio [32]. We note that the change of this parameter does not lead to significant quantitative and any qualitative changes of the results (see Appendix C for the details), and we comment on the possible choices for materials subsequently at the end of Sec. IV.

We consider the interaction between two s-type excitons with the same ($\{n,n'\} = 11,22,33$) and different ($\{n,n'\} = 12,23$) principal quantum numbers. The results of the calculation are plotted in Fig. 2. Figure 2(a) shows the direct-interaction term as a function of dimensionless transferred momentum for various scattering processes. We find that the direct interaction for ground-state excitons and excited excitons has the same qualitative behavior, dropping to zero

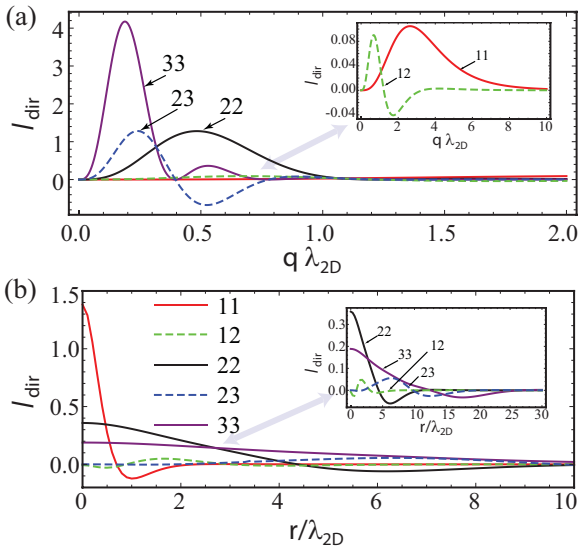

FIG. 2. Interaction of s excitons. (a) Dependence of the direct exciton-exciton interaction on the scattered wave vector q (in terms of reverse two-dimensional exciton radius). Hereafter, the dimensionless value of the integral is presented. The solid lines correspond to interaction of excitons with the same $\{n,n\}$ principal quantum number, while dashed lines correspond to the different $\{n,n'\}$ principal quantum numbers. (b) Real-space dependence of the direct-interaction integral.

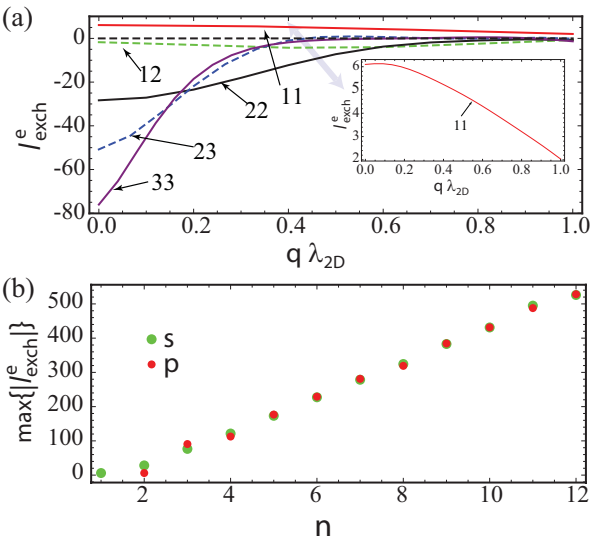

FIG. 3. (a) Dependence of the s-type exciton-exciton interaction electron exchange term on the scattered wave vector q. (b) The maximal absolute value of the exchange interaction plotted as a function of principal quantum number n for s and p states. The linear-in-n growth of the interaction strength is observed.

for small q and exhibiting a maximum for intermediate momenta. The position of the direct-interaction peak shifts to smaller transferred wave vectors for increasing n, and its magnitude increases radically. We check that the latter holds even for very large quantum numbers (up to $n = 10$; not shown). In Fig. 2(b) we plot a 2D Fourier transform of the $I_{\text{dir}}[q]$ interaction integral, which represents its real-space dependence. The curves depict maximal but finite interaction strength for $n = n' = 1$ excitons at a small separation, which rapidly decreases with r. For excited states the $r \to 0$ peak flattens out, while the total interaction range increases.

To understand the origin of the interaction we examined the large-r behavior of the potential for excitons with quantum number in the range $n = 3, \ldots, 10$ (see Appendix B for details). The analysis of the interaction tail unveiled the rapid increase of the interaction strength with the growth of the principal quantum number, which is another fingerprint of the long-range nature of the interaction [3,7,29]. The corresponding numerical fit of the real-space interaction dependence revealed the van der Waals nature of the potential ($I_{\text{dir}} \propto r^{-6}$), which was previously reported by Schindler and Zimmermann also for QW excitons in the ground state [33].

Next, we calculate the Coulomb exchange contribution to the s-type exciton-exciton interaction. Figure 3(a) illustrates the dependence of the exchange integral I_{exch} as a function of $\mathbf{q}$ for different states. For the ground-state scattering (inset, curve 11) the interaction is maximal in the $q \to 0$ region, decreasing for large transferred wave vectors and has a positive sign (repulsive potential). However, already for $n = n' = 2$ the sign of the exciton interaction changes to the *attractive* one, with a maximal absolute value at zero q. The same change applies to higher-excited-state interaction and also to cross scattering between ground- and excited-state excitons. Moreover, we note that the maximal absolute value of the potential grows with the principal quantum number n, representing an enhancement of the exchange contribution by an increase of the effective interaction area due to the spread of wave functions. Consequently, the real-space dependence of the exchange interaction has the form of an exponential decay, defined by the decrease of the wave-function overlap area.

Finally, we study the dependence of the maximal absolute value of the exchange integral as a function of the principal quantum number $n = n'$, measured at the $q \to 0$ point. The behavior is shown in Fig. 3(b) for both s and p excitons, corresponding to a linear increase of the magnitude for large principal quantum numbers, $n > 3$, where s and p interaction strengths coincide. At the same time, the clear difference in $\max\{|I^e_{\text{exch}}|\}$ for s and p states is visible in the $n \leqslant 3$ range. This result can be explained by the fact that the radial parts of the wave functions of excited states have the same shape at larger radii, despite being different at small r, relevant for small-n excitons.

The total interaction potential in the case of equal wave vectors and principal quantum numbers, represented by Eq. (8), is shown in Fig. 4 as a function of the transferred momentum $\mathbf{q}$. It reveals that for very small values of q the total interaction for excited states is fully determined by the exchange interaction, which is attractive. However, for larger transferred momenta it is replaced by weak repulsion, showing the dominant contribution of the direct-interaction term in the large-q region. Notably, for a higher excitation number the region dominated by repulsion is shifted to smaller transferred momenta values. This alternating-sign behavior is intriguing as it can potentially lead to the formation of a supersolid state [34].

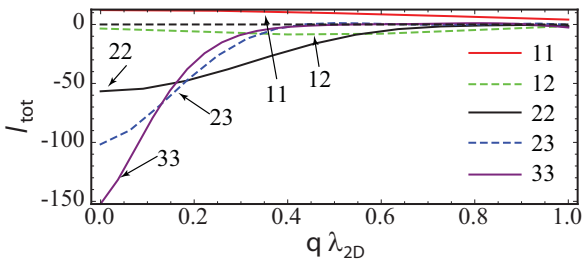

FIG. 4. Overall interaction of s-type excitons as a function of the scattered wave vector q. For small values of q the interaction of the excited states is highly attractive due to the dominant exchange interaction, while for large values the direct term prevails, leading to the weak repulsive character of total interaction.

B. Interaction between p-type excitons

We proceed with the discussion of direct and exchange Coulomb integrals for two p-type excitons. While nonzero angular momentum states are not straightforwardly accessed by optical means in direct-gap semiconductors (GaAs, GaN, ZnO, etc.), one can envisage the situation when these become relevant in the low-dimensional structures. As an example they can be created by two-photon pumping [35]. The results of numerical integrations are presented in Fig. 5. Figures 5(a) and 5(b) show the direct-interaction integral as a function of transferred momentum and interexciton distance for various values of the principal quantum number. We note that, qualitatively, it has the same behavior as s-type excitons, with minor variations of positions and heights of absolute maxima. Notably, while for p-shells of 3D excitons the long-range interaction has a dipole-dipole contribution, it is absent for 2D excitons with nonzero angular momentum.

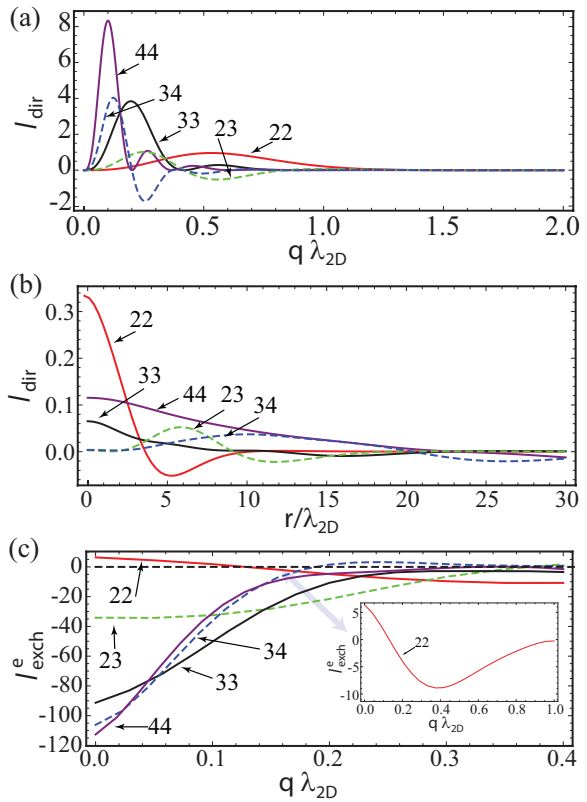

FIG. 5. Interaction of p excitons. (a) Dependence of the direct exciton-exciton interaction on the scattered wave vector q (in terms of reverse two-dimensional Bohr radius). Here, the dimensionless value of integration is presented. (b) Real-space dependence of the direct-interaction integral. (c) Dependence of the electron exchange term on the scattered wave vector q.

Finally, Fig. 5(c) illustrates the exchange-term dependence on the transferred wave vector $\mathbf{q}$. We first note that the minimal energy state of p excitons corresponds to the value of principal quantum number $n = 2$. Hence, the exchange interaction of $2p$ excitons is repulsive and similar to the interaction of $1s$ excitons. As for excited states, it has a shape similar to that of s-type excitons with a higher value of absolute maxima.

IV. DISCUSSION AND OUTLOOK

Previously, we have shown that interactions between excited excitonic states in 2D structures have different contributions, which are largely dependent on the main quantum number n and interexciton separation. While very large n excitons physics is expected to be driven by long-range interactions, the relevant properties of ground-state excitons are defined by the short-range exchange potential. Thus, we expect the crossover between regimes to happen in the range of intermediate $n > 1$, where strong short-range attractive interaction dominates. To increase the overall interaction even further, we consider possible semiconductor materials where Rydberg excitons can be observed. The parameters of the 2D Bohr radius, binding energy Ry_{3D}, the Coulomb interaction prefactor of Eq. (4) $\alpha_C \equiv e^2\lambda_{2D}/4\pi\varepsilon\varepsilon_0$, and the band gap E_g are collected in Table I for various semiconductors (data are taken from Refs. [36–38]). One can see that with increasing band gap the exciton Bohr radius decreases, consequently decreasing the interaction constant. At the same time we note that successful generation of highly excited excitonic states requires a large binding energy of excitons, which allows one to address separately excitonic states with large n. Therefore, an interplay between interaction strength and exciton energy separation determines the choice of materials relevant for the described physics. Depending on the goal, they may span from mid-band-gap semiconductors (e.g., GaAs)

TABLE I. The estimation of the Bohr radius of the two-dimensional exciton, Coulomb interaction constant $\alpha_C \equiv e^2\lambda_{2D}/4\pi\varepsilon\varepsilon_0$, and binding energy (3D) for direct-band-gap semiconductors. The list is sorted by increasing order of a semiconductor band gap.

	λ_{2D}(Å)	Ry_{3D} (meV)	α_C (μeVμm^2)	E_g (eV)
InAs	184.45	1.29	1.75	0.354
GaSb	111.95	2.05	1.03	0.726
InN	36.3	6.47	0.34	0.78
InP	46.95	6.13	0.54	1.344
GaAs	93.6	4.57	1.04	1.424
CdTe	30.1	11.70	0.42	1.5
GaN	21.75	17.04	0.32	3.2
ZnO	10.55	40.22	0.178	3.37

to wide-band-gap materials (e.g., GaN). Additionally, we underline the possible importance of materials with the non-Rydberg excitonic spectrum, represented by transition-metal dichalcogenides [39–42], where the described bound can be violated.

Finally, as optical selection rules does not forbid the creation of s excitonic states with different n, the mixtures of excitons with $n = 1,2,3,\ldots$ can be realized. Given its mutually attractive and repulsive interaction, we expect intriguing collective effects to appear in the system.

V. CONCLUSION

We studied the Coulomb interaction of excited states of excitons in direct-gap semiconductors. We showed that the total interaction of higher energy states has an attractive character due to the dominant contribution of exchange terms. A linear increase of interaction maxima with the increase of the principal quantum number of the excitonic state was observed. Contrary to 3D excitons, no dipolar interaction appears for large-quantum-number 2D excitons, and direct interaction has van der Waals behavior. The results point out the importance of Rydberg excitonic states and may open the way towards studies of repulsive-attractive bosonic mixtures.

ACKNOWLEDGMENTS

This work was supported by the FP7 ITN NOTEDEV network, RISE project 644076 CoExAN, the Russian Federal Target Program, project RFMEFI58715X0020, and the Singapore Ministry of Education under AcRF Tier 2 Grant No. MOE2015-T2-1-055. O.K. acknowledges the funding from the European Union Seventh Framework Programme through ERC Grant QIOS (Grant No. 306576). V.S. thanks the Niels Bohr Institute for hospitality.

APPENDIX A: DERIVATION OF MATRIX ELEMENTS FOR COULOMB SCATTERING OF RYDBERG EXCITONS

A two-dimensional exciton in the nl state with center-of-mass wave vector $\mathbf{Q}$ is described by wave functions (1) and (2) of the main text, corresponding to center-of-mass and internal motions, respectively. The spin degree of freedom can be introduced in the following way. The total angular momentum projection of the conduction electron on the growth axis is $s_e = \pm 1/2$. In the current work we restrict ourselves to the consideration of heavy-hole excitons. The angular momentum projection of heavy holes is $j_h = \pm 3/2$. Correspondingly, we have four independent heavy-hole exciton states: the dipole-active states $|J_z = \pm 1\rangle = |s_e = \mp 1/2, j_h = \pm 3/2\rangle$ and the dark states $|J_z = \pm 2\rangle = |s_e = \pm 1/2, j_h = \pm 3/2\rangle$. Further, in a general case an exciton state with total momentum $|S\rangle$ can be defined as $\chi_S(s_e, j_h) = \langle s_e, j_h | S\rangle$ (see, e.g., Ref. [19] for a detailed description).

We proceed by considering the Coulomb scattering of excitons. We are interested in the processes of elastic scattering which conserve total spin and principal quantum numbers of excitons. They correspond to the scattering process described as

$$(nl,\mathbf{Q},S) + (n'l,\mathbf{Q}',S) \rightarrow (nl,\mathbf{Q}+\mathbf{q},S) + (n'l,\mathbf{Q}'-\mathbf{q},S), \tag{A1}$$

where we defined a distinct exciton spin state $|S\rangle = |s, j\rangle$, yielding $\chi_S(s_e, j_h) = \langle s_e, j_h | S\rangle = \delta_{s_e,s}\delta_{j_h,j}$.

Within the Hartree-Fock approximation, the two-exciton initial state with the same spin is described by the following wave function:

$$\begin{aligned}
&\Phi^S_{\mathbf{Q}\mathbf{Q}'nn'}(\mathbf{r}_e,s_e,\mathbf{r}_h,j_h,\mathbf{r}_{e'},s_{e'},\mathbf{r}_{h'},j_{h'}) \\
&= \frac{1}{\sqrt{2}}\left\{\frac{1}{\sqrt{2}}[\Psi_{\mathbf{Q},n}(\mathbf{r}_e,\mathbf{r}_h)\chi_S(s_e,s_h)\Psi_{\mathbf{Q}',n'}(\mathbf{r}_{e'},\mathbf{r}_{h'})\chi_S(s_{e'},s_{h'}) + \Psi_{\mathbf{Q},n}(\mathbf{r}_{e'},\mathbf{r}_{h'})\chi_S(s_{e'},s_{h'})\Psi_{\mathbf{Q}',n'}(\mathbf{r}_e,\mathbf{r}_h)\chi_S(s_e,s_h)]\right. \\
&\quad \left. - \frac{1}{\sqrt{2}}[\Psi_{\mathbf{Q},n}(\mathbf{r}_{e'},\mathbf{r}_h)\chi_S(s_{e'},s_h)\Psi_{\mathbf{Q}',n'}(\mathbf{r}_e,\mathbf{r}_{h'})\chi_S(s_e,s_{h'}) + \Psi_{\mathbf{Q},n}(\mathbf{r}_e,\mathbf{r}_{h'})\chi_S(s_e,s_{h'})\Psi_{\mathbf{Q}',n'}(\mathbf{r}_{e'},\mathbf{r}_h)\chi_S(s_{e'},s_h)]\right\} \\
&= \delta_{s_e,s}\delta_{s_{e'},s}\delta_{j_h,j}\delta_{j_{h'},j}\left\{\frac{1}{2}[\Psi_{\mathbf{Q},n}(\mathbf{r}_e,\mathbf{r}_h)\Psi_{\mathbf{Q}',n'}(\mathbf{r}_{e'},\mathbf{r}_{h'}) + \Psi_{\mathbf{Q},n}(\mathbf{r}_{e'},\mathbf{r}_{h'})\Psi_{\mathbf{Q}',n'}(\mathbf{r}_e,\mathbf{r}_h)]\right. \\
&\quad \left. - \frac{1}{2}[\Psi_{\mathbf{Q},n}(\mathbf{r}_{e'},\mathbf{r}_h)\Psi_{\mathbf{Q}',n'}(\mathbf{r}_e,\mathbf{r}_{h'}) + \Psi_{\mathbf{Q},n}(\mathbf{r}_e,\mathbf{r}_{h'})\Psi_{\mathbf{Q}',n'}(\mathbf{r}_{e'},\mathbf{r}_h)]\right\}.
\end{aligned} \tag{A2}$$

The Hamiltonian can be written in the form

$$\hat{H} = \hat{H}_1(\mathbf{r}_e,\mathbf{r}_h) + \hat{H}_2(\mathbf{r}_{e'},\mathbf{r}_{h'}) + V_{\text{int}}(\mathbf{r}_e,\mathbf{r}_h,\mathbf{r}_{e'},\mathbf{r}_{h'}), \tag{A3}$$

where $\hat{H}_j$ corresponds to the energy of the jth exciton and V_{int} denotes the Coulomb interaction potential between particles.

The intraexciton terms read

$$\hat{H}_1(\mathbf{r}_e,\mathbf{r}_h) = -\frac{\hbar^2}{2m_e}\Delta_e - \frac{\hbar^2}{2m_h}\Delta_h - V(|\mathbf{r}_e - \mathbf{r}_h|), \tag{A4}$$

$$\hat{H}_2(\mathbf{r}_{e'},\mathbf{r}_{h'}) = -\frac{\hbar^2}{2m_e}\Delta_{e'} - \frac{\hbar^2}{2m_h}\Delta_{h'} - V(|\mathbf{r}_{e'} - \mathbf{r}_{h'}|), \tag{A5}$$

and each consists of kinetic- and potential-energy contributions. $V(r) = \frac{e^2}{4\pi\varepsilon_0\varepsilon r}$ corresponds to the Coulomb interaction energy, screened by the static dielectric constant ε; ε_0 is the vacuum permittivity.

The interexciton interaction part can be written as

$$V_{\text{int}}(\mathbf{r}_e,\mathbf{r}_h,\mathbf{r}_{e'},\mathbf{r}_{h'}) = -V(|\mathbf{r}_e-\mathbf{r}_{h'}|) - V(|\mathbf{r}_{e'}-\mathbf{r}_h|) + V(|\mathbf{r}_e-\mathbf{r}_{e'}|) + V(|\mathbf{r}_h-\mathbf{r}_{h'}|), \tag{A6}$$

where four possible interactions are accounted for. The scattering amplitude of the process described by Eq. (3) of the main text is given by the matrix element:

$$\begin{aligned}
H_{nn'mS}(\mathbf{Q},\mathbf{Q}',\mathbf{q}) &= \int d^2\mathbf{r}_e \sum_{s_e}\int d^2\mathbf{r}_h \sum_{j_h}\int d^2\mathbf{r}_{e'}\sum_{s_{e'}}\int d^2\mathbf{r}_{h'}\sum_{j_{h'}} \Phi^{*S}_{\mathbf{Q}\mathbf{Q}'nn'}(\mathbf{r}_e,s_e,\mathbf{r}_h,j_h,\mathbf{r}_{e'},s_{e'},\mathbf{r}_{h'},j_{h'}) \\
&\times V_{\text{int}}(\mathbf{r}_e,\mathbf{r}_h,\mathbf{r}_{e'},\mathbf{r}_{h'})\Phi^{S}_{\mathbf{Q}+\mathbf{q}\mathbf{Q}'-\mathbf{q}nn'}(\mathbf{r}_e,s_e,\mathbf{r}_h,j_h,\mathbf{r}_{e'},s_{e'},\mathbf{r}_{h'},j_{h'}) \\
&= \frac{1}{4}\delta_{s_e,s}\delta_{s_{e'},s}\delta_{j_h,j}\delta_{j_{h'},j} \\
&\times\Big[4\int d^2\mathbf{r}_e d^2\mathbf{r}_h d^2\mathbf{r}_{e'} d^2\mathbf{r}_{h'}\Psi^*_{\mathbf{Q},n}(\mathbf{r}_e,\mathbf{r}_h)\Psi^*_{\mathbf{Q}',n'}(\mathbf{r}_{e'},\mathbf{r}_{h'})V_{\text{int}}(\mathbf{r}_e,\mathbf{r}_h,\mathbf{r}_{e'},\mathbf{r}_{h'})\Psi_{\mathbf{Q}+\mathbf{q},n}(\mathbf{r}_e,\mathbf{r}_h)\Psi_{\mathbf{Q}'-\mathbf{q},n'}(\mathbf{r}_{e'},\mathbf{r}_{h'}) \\
&+4\int d^2\mathbf{r}_e d^2\mathbf{r}_h d^2\mathbf{r}_{e'} d^2\mathbf{r}_{h'}\Psi^*_{\mathbf{Q},n}(\mathbf{r}_e,\mathbf{r}_h)\Psi^*_{\mathbf{Q}',n'}(\mathbf{r}_{e'},\mathbf{r}_{h'})V_{\text{int}}(\mathbf{r}_e,\mathbf{r}_h,\mathbf{r}_{e'},\mathbf{r}_{h'})\Psi_{\mathbf{Q}+\mathbf{q},n}(\mathbf{r}_{e'},\mathbf{r}_{h'})\Psi_{\mathbf{Q}'-\mathbf{q},n'}(\mathbf{r}_e,\mathbf{r}_h) \\
&-4\int d^2\mathbf{r}_e d^2\mathbf{r}_h d^2\mathbf{r}_{e'} d^2\mathbf{r}_{h'}\Psi^*_{\mathbf{Q},n}(\mathbf{r}_e,\mathbf{r}_h)\Psi^*_{\mathbf{Q}',n'}(\mathbf{r}_{e'},\mathbf{r}_{h'})V_{\text{int}}(\mathbf{r}_e,\mathbf{r}_h,\mathbf{r}_{e'},\mathbf{r}_{h'})\Psi_{\mathbf{Q}+\mathbf{q},n}(\mathbf{r}_{e'},\mathbf{r}_h)\Psi_{\mathbf{Q}'-\mathbf{q},n'}(\mathbf{r}_e,\mathbf{r}_{h'}) \\
&-4\int d^2\mathbf{r}_e d^2\mathbf{r}_h d^2\mathbf{r}_{e'} d^2\mathbf{r}_{h'}\Psi^*_{\mathbf{Q},n}(\mathbf{r}_e,\mathbf{r}_h)\Psi^*_{\mathbf{Q}',n'}(\mathbf{r}_{e'},\mathbf{r}_{h'})V_{\text{int}}(\mathbf{r}_e,\mathbf{r}_h,\mathbf{r}_{e'},\mathbf{r}_{h'})\Psi_{\mathbf{Q}+\mathbf{q},n}(\mathbf{r}_e,\mathbf{r}_{h'})\Psi_{\mathbf{Q}'-\mathbf{q},n'}(\mathbf{r}_{e'},\mathbf{r}_h)\Big] \\
&= \delta_{s_e,s}\delta_{s_{e'},s}\delta_{j_h,j}\delta_{j_{h'},j}\big[H_{\text{dir}}(n,n',\mathbf{Q},\mathbf{Q}',\mathbf{q}) + H^X_{\text{exch}}(n,n',\mathbf{Q},\mathbf{Q}',\mathbf{q}) + H^e_{\text{exch}}(n,n',\mathbf{Q},\mathbf{Q}',\mathbf{q}) + H^h_{\text{exch}}(n,n',\mathbf{Q},\mathbf{Q}',\mathbf{q})\big],
\end{aligned} \tag{A7}$$

where four terms correspond to direct interaction, exciton exchange, electron exchange, and hole exchange. They can be written explicitly as

$$\begin{aligned}
H_{\text{dir}}(n,n',m,\mathbf{q}) &= \frac{\alpha_C}{A}I_{\text{dir}}(n,n',m,\mathbf{q}) = \frac{\alpha_C}{A}\frac{(n-|m|-1)!(n'-|m|-1)!}{2^4\pi^2(n-1/2)^3(n'-1/2)^3(n+|m|-1)!(n'+|m|-1)!}\frac{(2\pi)^3}{\lambda_{2\text{D}}q} \\
&\times\int_0^\infty\int_0^\infty[-J_0(\beta_h\lambda_{2\text{D}}qx)J_0(\beta_e\lambda_{2\text{D}}qx') - J_0(\beta_e\lambda_{2\text{D}}qx)J_0(\beta_h\lambda_{2\text{D}}qx') + J_0(\beta_h\lambda_{2\text{D}}qx)J_0(\beta_h\lambda_{2\text{D}}qx') \\
&+ J_0(\beta_e\lambda_{2\text{D}}qx)J_0(\beta_e\lambda_{2\text{D}}qx')]\left[\frac{x}{n-1/2}\right]^2 e^{-\frac{x}{n-1/2}} \\
&\times\left[L^{2|m|}_{n-|m|-1}\left(\frac{x}{n-1/2}\right)\right]^2 x dx\left[\frac{x'}{n'-1/2}\right]^2 e^{-\frac{x'}{n'-1/2}}\left[L^{2|m|}_{n'-|m|-1}\left(\frac{x'}{n'-1/2}\right)\right]^2 x' dx',
\end{aligned} \tag{A8}$$

$$\begin{aligned}
H^X_{\text{exch}}(n,n',m,\Delta\mathbf{Q},\mathbf{q}) &= \frac{\alpha_C}{A}I^X_{\text{exch}}(n,n',m,\Delta\mathbf{Q},\mathbf{q}) \\
&= \frac{\alpha_C}{A}\frac{(n-|m|-1)!(n'-|m|-1)!}{2^4\pi^2(n-1/2)^3(n'-1/2)^3(n+|m|-1)!(n'+|m|-1)!} \\
&\times\int d^2\mathbf{x}d^2\mathbf{y}_1d^2\mathbf{y}_2 e^{i(\Delta\mathbf{Q}-\mathbf{q})\lambda_{2\text{D}}[\beta_e\mathbf{y}_1+\beta_h\mathbf{y}_2+(\beta_h-\beta_e)\mathbf{x}]}\frac{x^2|\mathbf{y}_2-\mathbf{y}_1-\mathbf{x}|^2}{(n-1/2)^2(n'-1/2)^2}e^{-(x+|\mathbf{y}_2-\mathbf{y}_1-\mathbf{x}|)[\frac{1}{n-1/2}+\frac{1}{n'-1/2}]} \\
&\times L^{2|m|}_{n-|m|-1}\left(\frac{x}{n-1/2}\right)L^{2|m|}_{n'-|m|-1}\left(\frac{|\mathbf{y}_2-\mathbf{y}_1-\mathbf{x}|}{n'-1/2}\right)L^{2|m|}_{n-|m|-1}\left(\frac{|\mathbf{y}_2-\mathbf{y}_1-\mathbf{x}|}{n-1/2}\right) \\
&\times L^{2|m|}_{n'-|m|-1}\left(\frac{x}{n'-1/2}\right)\left[-\frac{1}{y_1}-\frac{1}{y_2}+\frac{1}{|\mathbf{y}_1+\mathbf{x}|}+\frac{1}{|\mathbf{y}_2-\mathbf{x}|}\right],
\end{aligned} \tag{A9}$$

$$\begin{aligned}
H^e_{\text{exch}}(n,n',m,\Delta\mathbf{Q},\mathbf{q}) &= \frac{\alpha_C}{A}I^e_{\text{exch}}(n,n',m,\Delta\mathbf{Q},\mathbf{q}) \\
&= -\frac{\alpha_C}{A}\frac{(n-|m|-1)!(n'-|m|-1)!}{2^4\pi^2(n-1/2)^3(n'-1/2)^3(n+|m|-1)!(n'+|m|-1)!} \\
&\times\int d^2\mathbf{x}d^2\mathbf{y}_1d^2\mathbf{y}_2 e^{i\beta_e\lambda_{2\text{D}}\Delta\mathbf{Q}(\mathbf{y}_1+\mathbf{x})}e^{i\lambda_{2\text{D}}\mathbf{q}[\beta_h\mathbf{y}_2-\beta_e\mathbf{y}_1-\mathbf{x}]}\left[\frac{x}{n-1/2}\frac{|\mathbf{y}_2-\mathbf{y}_1-\mathbf{x}|}{n'-1/2}\frac{y_1}{n-1/2}\frac{y_2}{n'-1/2}\right]^{|m|}
\end{aligned}$$

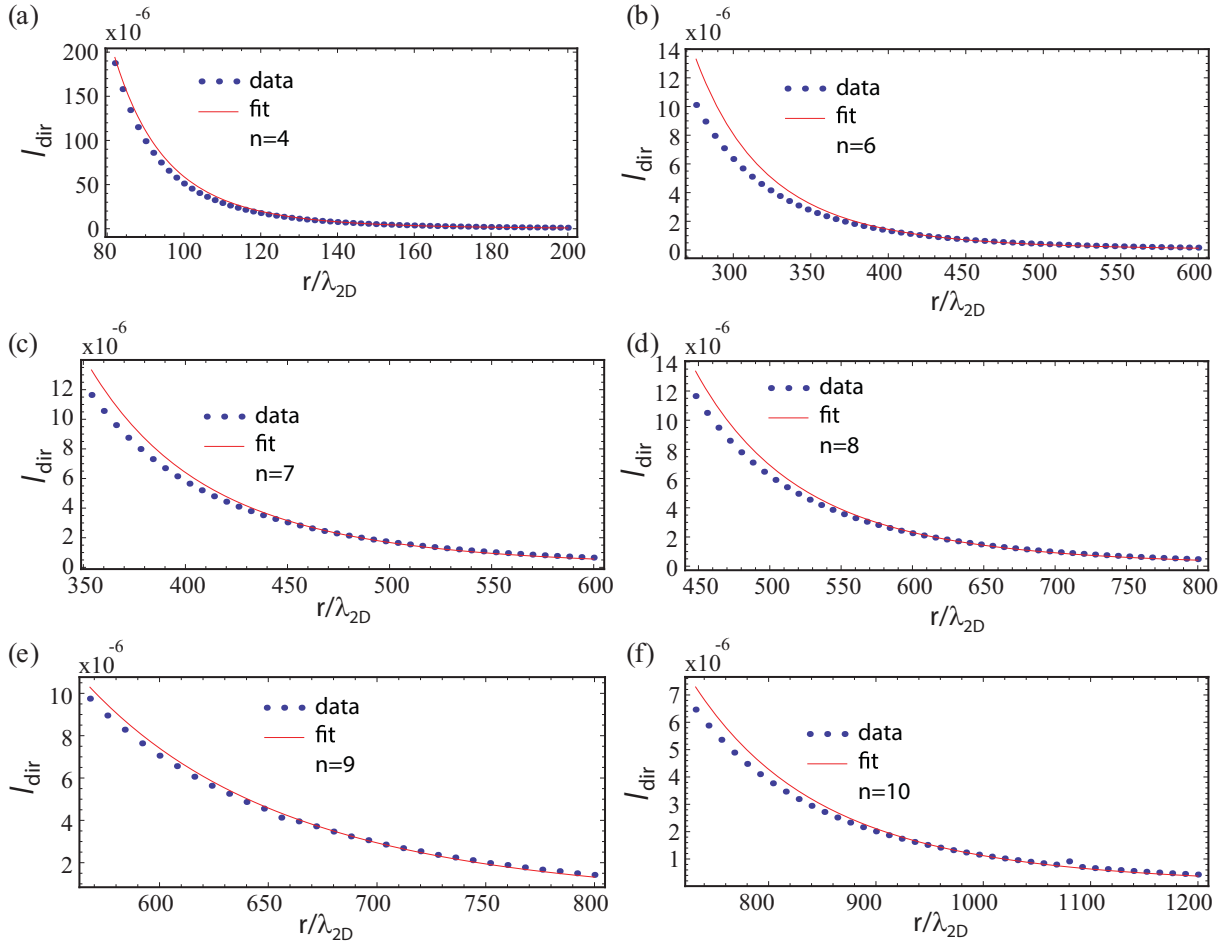

FIG. 6. Dependence of the long-range direct exciton-exciton interaction on the separation distance r. (a)–(f) correspond to the interaction of states with principal quantum number $n = 4,6,7,8,9,10$, respectively. For each value of n the numerical fit shows $\propto r^{-6}$ dependence, characteristic of van der Waals interaction.

$$\times e^{-\frac{x}{2n-1}} e^{-\frac{|\mathbf{y}_2-\mathbf{y}_1-\mathbf{x}|}{2n'-1}} e^{-\frac{y_1}{2n-1}} e^{-\frac{y_2}{2n'-1}} L^{2|m|}_{n-|m|-1}\left(\frac{x}{n-\frac{1}{2}}\right) L^{2|m|}_{n'-|m|-1}\left(\frac{|\mathbf{y}_2-\mathbf{y}_1-\mathbf{x}|}{n'-\frac{1}{2}}\right) L^{2|m|}_{n-|m|-1}\left(\frac{y_1}{n-\frac{1}{2}}\right)$$

$$\times L^{2|m|}_{n'-|m|-1}\left(\frac{y_2}{n'-\frac{1}{2}}\right)\left[-\frac{1}{y_2}-\frac{1}{y_1}+\frac{1}{|\mathbf{y}_1+\mathbf{x}|}+\frac{1}{|\mathbf{y}_2-\mathbf{x}|}\right], \tag{A10}$$

$$H^h_{\text{exch}}(n,n',m,\Delta\mathbf{Q},\mathbf{q}) = \frac{\alpha_C}{A} I^h_{\text{exch}}(n,n',m,\Delta\mathbf{Q},\mathbf{q})$$

$$= -\frac{\alpha_C}{A}\frac{(n-|m|-1)!(n'-|m|-1)!}{2^4\pi^2(n-1/2)^3(n'-1/2)^3(n+|m|-1)!(n'+|m|-1)!}$$

$$\times \int d^2\mathbf{x}d^2\mathbf{y}_1d^2\mathbf{y}_2 e^{i\beta_e\lambda_{2D}\Delta\mathbf{Q}(\mathbf{y}_2-\mathbf{x})} e^{i\lambda_{2D}\mathbf{q}[-\beta_h\mathbf{y}_2+\beta_e\mathbf{y}_1+\mathbf{x}]}\left[\frac{x}{n-1/2}\frac{|\mathbf{y}_2-\mathbf{y}_1-\mathbf{x}|}{n'-1/2}\frac{y_1}{n-1/2}\frac{y_2}{n'-1/2}\right]^{|m|}$$

$$\times e^{-\frac{x}{2n-1}} e^{-\frac{|\mathbf{y}_2-\mathbf{y}_1-\mathbf{x}|}{2n'-1}} e^{-\frac{y_1}{2n-1}} e^{-\frac{y_2}{2n'-1}} L^{2|m|}_{n-|m|-1}\left(\frac{x}{n-\frac{1}{2}}\right) L^{2|m|}_{n'-|m|-1}\left(\frac{|\mathbf{y}_2-\mathbf{y}_1-\mathbf{x}|}{n'-\frac{1}{2}}\right) L^{2|m|}_{n-|m|-1}\left(\frac{y_1}{n-\frac{1}{2}}\right)$$

$$\times L^{2|m|}_{n'-|m|-1}\left(\frac{y_2}{n'-\frac{1}{2}}\right)\left[-\frac{1}{y_2}-\frac{1}{y_1}+\frac{1}{|\mathbf{y}_1+\mathbf{x}|}+\frac{1}{|\mathbf{y}_2-\mathbf{x}|}\right], \tag{A11}$$

where we defined $\alpha_C \equiv e^2\lambda_{2D}/4\pi\varepsilon\varepsilon_0$.

In the derivation the following radius vector transformations were used: $\rho = \mathbf{r}_e - \mathbf{r}_h$, $\mathbf{R} = \beta_e\mathbf{r}_e + \beta_h\mathbf{r}_h$, $\rho' = \mathbf{r}_{e'} - \mathbf{r}_{h'}$, $\mathbf{R}' = \beta_e\mathbf{r}_{e'} + \beta_h\mathbf{r}_{h'}$, $\xi = \mathbf{R} - \mathbf{R}'$, $\sigma = \frac{\mathbf{R}+\mathbf{R}'}{2}$, $\Delta\mathbf{Q} = \mathbf{Q}' - \mathbf{Q}$, $\mathbf{x} = \frac{\rho}{\lambda_{2D}}$, $\mathbf{x}' = \frac{\rho'}{\lambda_{2D}}$, $\mathbf{y}_1 = \frac{\xi-\beta_e\rho-\beta_h\rho'}{\lambda_{2D}}$, $\mathbf{y}_2 = \frac{\xi+\beta_h\rho+\beta_e\rho'}{\lambda_{2D}}$.

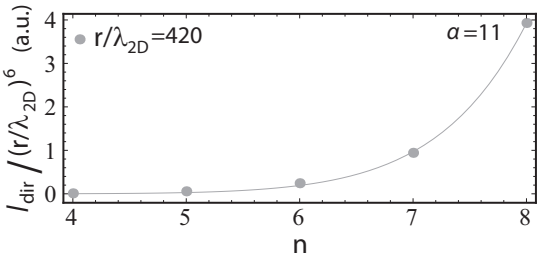

FIG. 7. Dependence of direct Coulomb interaction on the excitation number n for fixed separation distance. The numerical fit shows $\propto n^{\alpha}$ dependence.

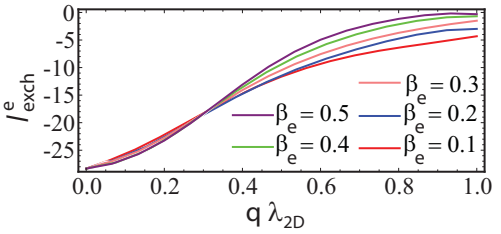

FIG. 8. Dependence of the exchange Coulomb interaction on the transferred momentum q for various fixed mass ratios $\beta_e = \{0.1,0.2,0.3,0.4,0.5\}$. We consider the interaction of two $2s$ excitons.

APPENDIX B: LONG-RANGE INTERACTION

This appendix is devoted to a detailed study of the long-range behavior of exciton-exciton direct interaction. For different values of the principal quantum number n we examine the real-space dependence at very large separation distances. The results are presented in Fig. 6. The numerical fits show the $I_{\rm dir} \propto r^{-6}$ dependence for interactions of excitons with various quantum numbers n. This confirms the van der Waals long-range behavior of the interaction potential. As expected, the distance where the van der Waals behavior becomes relevant rapidly grows with the increase of the principal quantum number.

The characteristic feature of the van der Waals interaction is the power dependence on the excitation number. To check this, we examined the dependence of the direct-interaction strength on the excitation number for different fixed values of the separation distance. The sample of results is presented in Fig. 7, where the power dependence $\propto n^{\alpha}$ is clearly seen. We observe that due to small number of points the power α can lie in the 7 to 12 range, and expect it to be equal $\alpha = 11$ if large n are considered.

APPENDIX C: EXCHANGE INTERACTION DEPENDENCE ON EFFECTIVE-MASS RATIO

As mentioned above, the exchange interaction between excited 2D excitonic states is strongly attractive and does not drastically depend on the electron-to-exciton mass ratio β_e. To prove this, we calculate the momentum dependence of the exchange interaction of $2s$ excitons for various values of β_e. The results are presented in Fig. 8. As can be seen, for relatively small values of transferred momenta the scattering amplitude has weak mass dependence.

[1] I. Bloch, J. Dalibard, and W. Zwerger, Many-body physics with ultracold gases, Rev. Mod. Phys. **80**, 885 (2008).

[2] C. Chin, R. Grimm, P. Julienne, and E. Tiesinga, Feshbach resonances in ultracold gases, Rev. Mod. Phys. **82**, 1225 (2010).

[3] T. F. Gallagher, *Rydberg Atoms* (Cambridge University Press, New York, 1994).

[4] M. D. Lukin, M. Fleischhauer, R. Cote, L. M. Duan, D. Jaksch, J. I. Cirac, and P. Zoller, Dipole Blockade and Quantum Information Processing in Mesoscopic Atomic Ensembles, Phys. Rev. Lett. **87**, 037901 (2001).

[5] A. Gaëtan, Y. Miroshnychenko, T. Wilk, A. Chotia, M. Viteau, D. Comparat, P. Pillet, A. Browaeys, and Ph. Grangier, Observation of collective excitation of two individual atoms in the Rydberg blockade regime, Nat. Phys. **5**, 115 (2009).

[6] E. Urban, T. A. Johnson, T. Henage, L. Isenhower, D. D. Yavuz, T. G. Walker, and M. Saffman, Observation of Rydberg blockade between two atoms, Nat. Phys. **5**, 110 (2009).

[7] M. Saffman, T. G. Walker, and K. Mølmer, Quantum information with Rydberg atoms, Rev. Mod. Phys. **82**, 2313 (2010).

[8] T. Peyronel, O. Firstenberg, Q.-Y. Liang, S. Hofferberth, A. V. Gorshkov, T. Pohl, M. D. Lukin, and V. Vuletić, Quantum nonlinear optics with single photons enabled by strongly interacting atoms, Nature (London) **488**, 57 (2012).

[9] O. Firstenberg, T. Peyronel, Q.-Y. Liang, A. V. Gorshkov, M. D. Lukin, and V. Vuletić, Attractive photons in a quantum nonlinear medium, Nature (London) **502**, 71 (2013).

[10] P. Schauß, M. Cheneau, M. Endres, T. Fukuhara, S. Hild, A. Omran, T. Pohl, C. Gross, S. Kuhr, and I. Bloch, Observation of spatially ordered structures in a two-dimensional Rydberg gas, Nature (London) **491**, 87 (2012).

[11] L. V. Butov, Cold exciton gases in coupled quantum well structures, J. Phys. Condens. Matter **19**, 295202 (2007).

[12] A. A. High, J. R. Leonard, A. T. Hammack, M. M. Fogler, L. V. Butov, A. V. Kavokin, K. L. Campman, and A. C. Gossard, Spontaneous coherence in a cold exciton gas, Nature (London) **483**, 584 (2012).

[13] I. Carusotto and C. Ciuti, Quantum fluids of light, Rev. Mod. Phys. **85**, 299 (2013).

[14] J. Kasprzak, M. Richard, S. Kundermann, A. Baas, P. Jeambrun, J. M. J. Keeling, F. M. Marchetti, M. H. Szymanska, R. Andre, J. L. Staehli, V. Savona, P. B. Littlewood, B. Deveaud, and L. S. Dang, Bose-Einstein condensation of exciton polaritons, Nature (London) **443**, 409 (2006).

[15] C. Schneider *et al.*, An electrically pumped polariton laser, Nature (London) **497**, 348 (2013).

[16] K. G. Lagoudakis, M. Wouters, M. Richard, A. Baas, I. Carusotto, R. André, L. S. Dang, and B. Deveaud-Plédran, Quantized vortices in an exciton-polariton condensate, Nat. Phys. **4**, 706 (2008).

[17] M. Sich, D. N. Krizhanovskii, M. S. Skolnick, A. V. Gorbach, R. Hartley, D. V. Skryabin, E. A. Cerda-Méndez, K. Biermann, R.

Hey, and P. V. Santos, Observation of bright polariton solitons in a semiconductor microcavity, Nat. Photonics **6**, 50 (2012).

[18] A. Amo, S. Pigeon, D. Sanvitto, V. G. Sala, R. Hivet, I. Carusotto, F. Pisanello, G. Leménager, R. Houdré, E. Giacobino, C. Ciuti, and A. Bramati, Polariton superfluids reveal quantum hydrodynamic solitons, Science **332**, 1167 (2011).

[19] C. Ciuti, V. Savona, C. Piermarocchi, A. Quattropani, and P. Schwendimann, Role of the exchange of carriers in elastic exciton-exciton scattering in quantum wells, Phys. Rev. B **58**, 7926 (1998).

[20] F. Tassone and Y. Yamamoto, Exciton-exciton scattering dynamics in a semiconductor microcavity and stimulated scattering into polaritons, Phys. Rev. B **59**, 10830 (1999).

[21] T. C. H. Liew and V. Savona, Single Photons from Coupled Quantum Modes, Phys. Rev. Lett. **104**, 183601 (2010).

[22] O. Kyriienko and T. C. H. Liew, Triggered single-photon emitters based on stimulated parametric scattering in weakly nonlinear systems, Phys. Rev. A **90**, 063805 (2014).

[23] O. Kyriienko, I. A. Shelykh, and T. C. H. Liew, Tunable single-photon emission from dipolaritons, Phys. Rev. A **90**, 033807 (2014).

[24] P. Cristofolini, G. Christmann, S. I. Tsintzos, G. Deligeorgis, G. Konstantinidis, Z. Hatzopoulos, P. G. Savvidis, and J. J. Baumberg, Coupling quantum tunneling with cavity photons, Science **336**, 704 (2012).

[25] G. Christmann, A. Askitopoulos, G. Deligeorgis, Z. Hatzopoulos, S. I. Tsintzos, P. G. Savvidis, and J. J. Baumberg, Oriented polaritons in strongly-coupled asymmetric double quantum well microcavities, Appl. Phys. Lett. **98**, 081111 (2011).

[26] K. Kristinsson, O. Kyriienko, and I. A. Shelykh, Terahertz laser based on dipolaritons, Phys. Rev. A **89**, 023836 (2014).

[27] M. Wouters, Resonant polariton-polariton scattering in semiconductor microcavities, Phys. Rev. B **76**, 045319 (2007).

[28] N. Takemura, S. Trebaol, M. Wouters, M. T. Portella-Oberli, and B. Deveaud, Polaritonic Feshbach resonance, Nat. Phys. **10**, 500 (2014).

[29] T. Kazimierczuk, D. Fröhlich, S. Scheel, H. Stolz and M. Bayer, Giant Rydberg excitons in the copper oxide Cu_2O, Nature (London) **514**, 343 (2014).

[30] D. G. W. Parfitt and M. E. Portnoi, The two-dimensional hydrogen atom revisited, J. Math. Phys. **43**, 4681 (2002).

[31] T. Hahn, CUBA multidimensional integrations, Comput. Phys. Commun. **168**, 78 (2005).

[32] P. Pfeffer and W. Zawadzki, Conduction electrons in GaAs: Five-level $k \cdot p$ theory and polaron effects, Phys. Rev. B **41**, 1561 (1990).

[33] C. Schindler and R. Zimmermann, Analysis of the exciton-exciton interaction in semiconductor quantum wells, Phys. Rev. B **78**, 045313 (2008).

[34] M. Matuszewski, T. Taylor, and A. V. Kavokin, Exciton Supersolidity in Hybrid Bose-Fermi Systems, Phys. Rev. Lett. **108**, 060401 (2012).

[35] G. Lemenager, F. Pisanello, J. Bloch, A. Kavokin, A. Amo, A. Lemaitre, E. Galopin, I. Sagnes, M. De Vittorio, E. Giacobino, and A. Bramati, Opt. Lett. **39**, 307 (2014).

[36] T. Hanada, Basic Properties of ZnO, GaN, and Related Materials, in *Oxide and Nitride Semiconductors*, Advances in Materials Research, Vol. 12, edited by T. Yao and S. Hong (Springer, Berlin, 2009), pp. 1–19.

[37] J. Singh, *Physics of Semiconductors and Their Heterostructures* (McGraw-Hill, New York, 1993).

[38] A. Rubio-Ponce, D. Olguín, and I. Hernández-Calderón, Calculation of the effective masses of II-VI semiconductor compounds, Superficies y Vacio **16**, 26 (2003).

[39] A. Chernikov, T. C. Berkelbach, H. M. Hill, A. Rigosi, Y. Li, O. B. Aslan, D. R. Reichman, M. S. Hybertsen, and T. F. Heinz, Exciton Binding Energy and Nonhydrogenic Rydberg Series in Monolayer WS_2, Phys. Rev. Lett. **113**, 076802 (2014).

[40] G. Berghauser and E. Malic, Analytical approach to excitonic properties of MoS_2, Phys. Rev. B **89**, 125309 (2014).

[41] D. Y. Qiu, F. H. da Jornada, and St. G. Louie, Optical Spectrum of MoS_2: Many-Body Effects and Diversity of Exciton States, Phys. Rev. Lett. **111**, 216805 (2013).

[42] T. Berkelbach, M. Hybertsen, and D. Reichman, Theory of neutral and charged excitons in monolayer transition metal dichalcogenides, Phys. Rev. B **88**, 045318 (2013).